

Error-tolerant multiqubit holonomic entangling gates

Jin-Lei Wu¹, Yan Wang¹, Jin-Xuan Han¹, Yongyuan Jiang¹, Jie Song¹, Yan Xia⁴, Shi-Lei Su², Weibin Li³

¹School of Physics, Harbin Institute of Technology, Harbin 150001, China

²School of Physics, Zhengzhou University, Zhengzhou 450001, China

³School of Physics and Astronomy, University of Nottingham, Nottingham NG7 2RD, United Kingdom

⁴Department of Physics, Fuzhou University, Fuzhou 350002, China

Nonadiabatic holonomic quantum computation, focusing mainly on implementing universal single- and two-qubit gates, commonly suffers gate fidelity losses inevitably due to the presence of systematic errors. Here we propose to realize fast holonomic multiqubit controlled (C_N -NOT) Rydberg atom gates. Uniquely, the gate time is independent of the control qubit number N . We show that the fast gate is largely immune to laser parameter fluctuations and motional dephasing. The high tolerance of systematic errors can be further enhanced through optimal pulse engineering. The proposed protocol is intrinsically different from typical schemes based on Rydberg blockade or antiblockade, and moreover can be implemented alternatively with superconducting circuits. Our study paves a new way to build robust multiqubit gates with Rydberg atoms trapped in optical arrays or superconducting circuits, and hence contributes to current efforts in developing scalable quantum computation with trapped atoms and fabricable superconducting devices.

Introduction.—Entangling gates based on geometric phases [1, 2] are immune to local fluctuations [3, 4], and therefore advantageous in realizing large scale quantum computation. Inspired by the adiabatic paradigms [5–7], protocols of nonadiabatic holonomic quantum computation (NHQC) are proposed [8–11], and have attracted growing interest and stimulated experimental demonstrations with superconducting artificial atoms [12], nuclear magnetic resonance [13], and diamond nitrogen-vacancy centers [14, 15]. Recent experiments also demonstrated highly efficient single-loop NHQC gates [16–20] and shortcut-to-adiabatic holonomic gates [21, 22]. Furthermore, multiqubit gates may be of great significance for realizing highly efficient lengthy quantum algorithms in quantum computation [23–28] and simulation [29–32]. The prevalent fashion of executing multiqubit holonomic gates is to decompose them into universal single- and two-qubit gates [34]. This approach, however, becomes extremely complicated when increasing the number of qubits [25] and inefficient due to multiple accumulation of decoherence and of systematic errors, such as fluctuations of laser parameters and qubit locations.

In this work, we propose a *one step* approach to implementing $(N + 1)$ -qubit holonomic gates [$(N + 1)$ -QHG] with either Rydberg atoms or superconducting circuits. We first focus on implementing $(N + 1)$ -QHGs with Rydberg atoms in optical array settings [35–37]. We identify a peculiar regime where the Rydberg antiblockade condition is employed but the blockade phenomenon emerges. Importantly, we show that the error sensitivity to fluctuations in laser parameters and interatomic distances can be suppressed through pulse engineering. Surprisingly, we find that the gate time is independent of N . Moreover, we show that $(N + 1)$ -QHGs can be implemented with high fidelities alternatively with superconducting circuits. Our study paves a route to achieve optimized holonomic quantum computation (OHQC) with

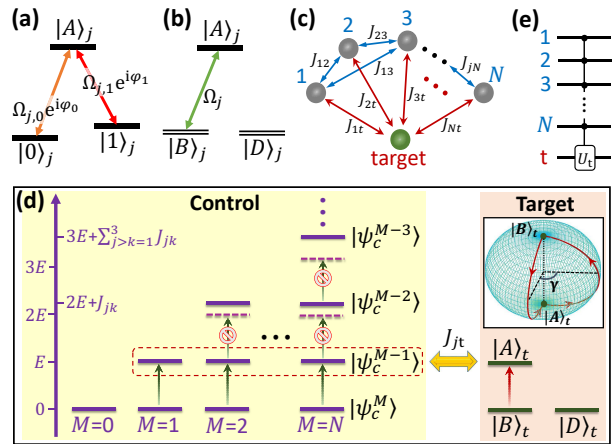


FIG. 1. (a) Level diagram. The j -th qubit consists of two states $|0\rangle_j$ and $|1\rangle_j$, coupled resonantly to an auxiliary state $|A\rangle_j$ with complex Rabi frequencies $\Omega_{j,0}e^{i\varphi_{j,0}}$ and $\Omega_{j,1}e^{i\varphi_{j,1}}$. (b) Dressed states $|D\rangle_j$ and $|B\rangle_j$. The latter couples to state $|A\rangle_j$ with Rabi frequency $\Omega_j = \sqrt{\Omega_{j,0}^2 + \Omega_{j,1}^2}$. (c) Ising-like (density-density) two-body interaction. The interaction between j and k -th qubits is J_{jk} . (d) Coupling between collective states of the control qubits (left panel). Bare energy in state $|A\rangle$ is E . Energies of the collective state with two or more excitation are shifted from resonance. The strong control-target qubit interaction allows to realize a geometric gate in a single step (right panel). Phase trajectory is illustrated on the Bloch sphere. (e) Circuit diagram of the $(N + 1)$ -qubit controlled- U_t gate. See text for details.

strongly interacting Rydberg atoms and superconducting circuits, and finds applications in quantum computation and simulations with multiple qubits.

Many-body model.—We consider a many-body setting of $(N + 1)$ qubits in which states of a single target qubit depend on N control qubits. Laser fields resonantly couple computational states $|0\rangle_j, |1\rangle_j$ to an auxiliary state $|A\rangle_j$ with complex Rabi frequencies $\Omega_{j,0}e^{i\varphi_{j,0}}$

and $\Omega_{j,1}e^{i\varphi_{j,1}}$ (phases $\varphi_{j,0}$ and $\varphi_{j,1}$) of the j -th qubit, as depicted in Fig. 1(a). The qubit states form dressed state $|B\rangle_j \equiv \sin(\theta_j/2)|0\rangle_j - \cos(\theta_j/2)e^{i\phi_j}|1\rangle_j$ [8], which is coupled to $|A\rangle_j$ with a laser field, while the other dressed state $|D\rangle_j \equiv \cos(\theta_j/2)|0\rangle_j + \sin(\theta_j/2)e^{i\phi_j}|1\rangle_j$ is not affected by this coupling laser [see Fig. 1(b)]. Here $\theta_j \equiv 2 \arctan(\Omega_{j,0}/\Omega_{j,1})$ and $\phi_j \equiv \varphi_{j,1} - \varphi_{j,0} - \pi$. In the following, we will mainly work in the $\{|A\rangle_j, |B\rangle_j\}$ basis.

In our setting the N control qubits are resonantly driven by a common control field (Rabi frequency Ω_c), and the target qubit by an operation field (Rabi frequency Ω_t). The respective coupling is described by Hamiltonian ($\hbar \equiv 1$): $\hat{H}_c = \frac{\Omega_c}{2} \sum_{j=1}^N \hat{\sigma}_j^x$ and $\hat{H}_t = \frac{\Omega_t}{2} \hat{\sigma}_t^x$, with $\hat{\sigma}^\xi$ ($\xi = x, y, z$) being the Pauli operator. We assume that the $(N+1)$ qubits are coupled to each other through Ising-like Hamiltonian, $\hat{H}_{\text{Ising}} = \sum_{j>k=1}^N (J_{jk} \hat{n}_j \hat{n}_k + J_{jt} \hat{n}_j \hat{n}_t)$, where J_{jk} is the interaction potential of the j -th and k -th qubits, as depicted in Fig. 1(c). $\hat{n}_j \equiv (\hat{\sigma}_j^z + \hat{I})/2$ with \hat{I} being the identity operator. The total Hamiltonian is given by $\hat{H} = \hat{H}_c + \hat{H}_t + \hat{H}_{\text{Ising}}$. The realization of this Hamiltonian will be discussed in latter sections.

When the Ising interaction is strong, many-body entanglement is induced in the dynamics. To this end, we define collective states of the control qubit $|\psi_c^K\rangle \equiv |B\rangle^K |A\rangle^{M-K}$ with integers $0 \leq K \leq M \leq N$, where numbers of control qubits in states $|D\rangle$, $|B\rangle$, and $|A\rangle$ are $(N-M)$, K , and $(M-K)$, respectively. The collective states $|\psi_c^K\rangle$ and $|\psi_c^{K-1}\rangle$ ($K \geq 1$) are coupled by the control field. The composite basis of the control and target qubits are $|\chi_1^K\rangle \equiv |\psi_c^K\rangle |B\rangle_t$, $|\chi_2^K\rangle \equiv |\psi_c^K\rangle |A\rangle_t$, $|\chi_3^K\rangle \equiv |\psi_c^{K-1}\rangle |B\rangle_t$, and $|\chi_4^K\rangle \equiv |\psi_c^{K-1}\rangle |A\rangle_t$. The Ising-like interaction energy of state $|\chi_i^K\rangle$ is $E_i^K = \sum_{j>k=1}^{M-K+\delta_{i3}+\delta_{i4}} [J_{jk} + (\delta_{i2} + \delta_{i4}) J_{jt}]$, where $\delta_{il'}$ is the Kronecker delta function and the subscript j (k) denotes the j -th (k -th) entry over the control qubits in $|A\rangle$. The Hamiltonian can be rewritten in terms of the composite states

$$\hat{H} = \sum_{M=0}^N \sum_{K=0}^M \left[\frac{\sqrt{K}\Omega_c}{2} \left(\hat{S}_{31}^K e^{it\Delta_{31}^K} + \hat{S}_{42}^K e^{it\Delta_{42}^K} \right) + \frac{\Omega_t}{2} \left(\hat{S}_{21}^K e^{it\Delta_{21}^K} + \hat{S}_{43}^K e^{it\Delta_{43}^K} \right) \right] + \text{H.c.}, \quad (1)$$

where $\hat{S}_{jk}^K = \hat{S}_{kj}^{K\dagger} = |\chi_j^K\rangle \langle \chi_k^K|$ with $\{j, k\} = \{1, 2, 3, 4\}$ is the collective transition operator, and $\Delta_{jk}^K = -\Delta_{kj}^K = E_j^K - E_k^K$ is the detuning. One can verify that the detuning $|\Delta_{jk}^K|$ increases with the number $(M-K)$ of qubits in state $|A\rangle$. In the strong interaction regime we set $|\Delta_{jk}^K| \gg \max\{|\Omega_c|, |\Omega_t|\}$ when $M \neq K$. We can keep terms with $K = M$, leading to an approximate Hamiltonian $\hat{H}' = \sum_{M=0}^N \left[\frac{\sqrt{M}\Omega_c}{2} (\hat{S}_{31}^M + \hat{S}_{42}^M e^{itJ_{jt}}) + \frac{\Omega_t}{2} (\hat{S}_{21}^M + \hat{S}_{43}^M e^{itJ_{jt}}) \right] + \text{H.c.}$, while highly oscillating terms for $K \neq M$ are neglected. The approximate Hamiltonian indicates that composite states with two or more

control qubits in $|A\rangle$ can be shifted from resonance, as illustrated in Fig. 1(d), and hence play negligible roles in the dynamics.

Multiqubit holonomic quantum gates.—We consider an identical control-target interaction $J_{jt} = J_0$ and an amplitude-modulated control field $\Omega_c = \Omega_m \cos \omega t$, with Ω_m being the amplitude and ω the modulation frequency. In the strong interaction regime and for parameters $|\omega| = |J_0| \gg \sqrt{N}|\Omega_m|/4$ and $|\Omega_m|/2 \gg |\Omega_t|$, the evolution of the $(N+1)$ -qubit system is dominated by an effective Hamiltonian,

$$\hat{H}_e = \left(\bigotimes_j^N |D\rangle_j \langle D| \right) \otimes \hat{H}_t. \quad (2)$$

Derivation of Eq. (2) can be found in the Supplemental Material (SM) [38]. Equation (2) shows that states of the target qubit are affected by the operation field only when all the control qubits populate in state $|D\rangle$. Otherwise, the evolution of the $(N+1)$ qubits is frozen. This gives a controlled $(N+1)$ -QHG, as long as a single-qubit holonomic gate \hat{U}_t on the target qubit is achieved. The gate corresponding to this situation is depicted in Fig. 1(e).

To implement the holonomic operation on the target qubit, state $|B\rangle_t$ experiences a cyclic evolution and obtains a purely geometric phase γ [8–20], while $|D\rangle_t$ state remains unchanged [see the Bloch sphere in Fig. 1(d)]. This corresponds to an arbitrary operation $\hat{U}_t(\theta, \phi, \gamma) = \exp(i\frac{\gamma}{2}) \exp(-i\frac{\gamma}{2} \mathbf{n} \cdot \boldsymbol{\sigma})$ on $\{|0\rangle_t, |1\rangle_t\}$ [38], where $\mathbf{n} = (\sin \theta \cos \phi, \sin \theta \sin \phi, \cos \theta)$ and $\boldsymbol{\sigma}$ contains the three standard Pauli operators. One can implement flexibly not only a universal set of holonomic gates of single ($N = 0$) and two ($N = 1$) qubit gates, but also direct multiqubit gates when $N \geq 2$.

Realization with Rydberg atoms.—Strong and long-range Rydberg-Rydberg interactions (RRI) between neutral atoms give rise to the Ising-like couplings of qubits [53, 54]. The RRI can be precisely controlled with Rydberg atoms trapped in optical tweezer arrays [36, 37, 43, 55]. Rydberg atoms interact with each other through the van der Waals interaction, $V_{jk} = C_6/R_{ij}^6$, C_6 being the interaction coefficient and R_{ij} the separation between the j -th and k -th Rydberg atoms. Note that dipole-dipole exchange interactions can also be applied to implement the scheme (See realization with superconducting circuit in SM [38]). To realize the identical control-target interaction, we consider a 2D array where the control atoms sit on a ring and the target atom in the center, as depicted in Fig. 2(a). We specify $|B\rangle_j = |0\rangle_j$ and $|D\rangle_j = |1\rangle_j$ for all control atoms. The auxiliary state is a Rydberg state $|r\rangle$. Dynamics of the system is governed by the Hamiltonian,

$$\hat{H}_I = \hat{H}_c + \hat{H}_t + \hat{H}_i. \quad (3)$$

where $\hat{H}_c = \sum_{j=1}^N \frac{\Omega_c}{2} |0\rangle_j \langle r| + \text{H.c.}$ and $\hat{H}_t = \sum_{j=0,1} \frac{\Omega_t}{2} e^{i\varphi_j} |j\rangle_t \langle r| + \text{H.c.}$ describe resonant laser cou-

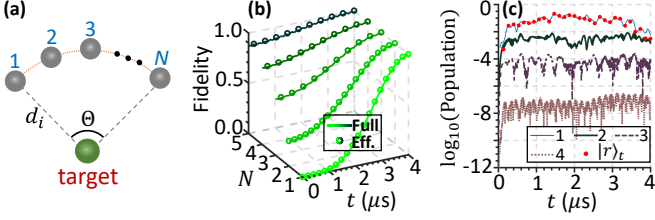


FIG. 2. (a) Spatial distribution of Rydberg atoms. $\Theta = \pi/2$ and $d_i = 9.6 \mu\text{m}$. (b) Fidelity evolution for performing a C_N -NOT gate of NHQC based on the full (solid lines) and effective (circles) Hamiltonian. Excellent agreement is obtained. (c) Population of collective states with different excitation numbers. We implement the C_3 -NOT gate with four atoms. The dotted red line denotes the population of the target atom in $|r\rangle_t$. The strong interaction prohibits multiple excitation during the gate evolution. $\Omega_m/2\pi = 10 \text{ MHz}$ and $\Omega_t/2\pi = 0.25 \text{ MHz}$. Other parameters can be found in the text.

pling of the control and target atoms, respectively. The RRI is given by $\hat{H}_i = \sum_{j>k=1}^N (V_{jk}|rr\rangle_{jk}\langle rr| + V_{jt}|rr\rangle_{jt}\langle rr|)$ [55–57].

To be concrete, we consider ^{87}Rb atoms and choose two hyperfine electronic ground states to encode computational states $|0\rangle \equiv |5S_{1/2}, F = 1, m_F = 1\rangle$ and $|1\rangle \equiv |5S_{1/2}, F = 2, m_F = 2\rangle$. The auxiliary Rydberg state is chosen as $|r\rangle \equiv |100S_{1/2}\rangle$ with $C_6/2\pi = 56.197 \text{ THz} \cdot \mu\text{m}^6$. The transition $|0\rangle(|1\rangle) \leftrightarrow |r\rangle$ can be achieved through a two-photon process [38], as demonstrated in recent experiments [41–44]. The control-target interatomic distance is $d_i = 9.6 \mu\text{m}$ to achieve strong interactions with $V_{jt}/2\pi = 71.79 \text{ MHz}$. Rabi frequencies Ω_m and Ω_t are chosen appropriately, depending on N , to satisfy $\omega = V_{jt} \gg \sqrt{N}|\Omega_m|/4$ and $|\Omega_m|/2 \gg |\Omega_t|$. With these conditions, we obtain an effective Hamiltonian $\hat{H}'_I = \left(\bigotimes_j^N |1\rangle_j\langle 1|\right) \otimes \hat{H}'_t$ with $\hat{H}'_t = \frac{\Omega_t}{2}\hat{\sigma}_t^x$ in the basis $\{|B\rangle_t, |r\rangle_t\}$. The effective Hamiltonian \hat{H}'_I , equivalent to Hamiltonian (2), will be the basis to implementing multi-qubit gate with Rydberg atoms.

In the following, we show that the effective Hamiltonian can accurately capture the dynamics. This will be demonstrated to realize a C_N -NOT gate [25, 28]. The figure of merit is the fidelity defined by $F = |\langle \Psi_i | \Psi(t) \rangle|^2$, where $|\Psi_i\rangle$ is an ideal state after a C_N -NOT gate on the initial state $|\Psi_0\rangle = \bigotimes_j^N (|0\rangle_j - |1\rangle_j) \otimes (|0\rangle_t - |1\rangle_t)/\sqrt{2^{N+1}}$ (also used for all later figures). The actual state $|\Psi(t)\rangle$ is obtained by solving the Schrödinger equation. An important result is that the full Hamiltonian \hat{H}_I and the effective Hamiltonian \hat{H}'_I produce nearly identical fidelities, as shown in Fig. 2(b). The excellent agreement in the fidelity results from the fact that two- or more-excitation states are strongly suppressed [Fig. 2(c)], validating the approximations used to derive the effective Hamiltonian.

We point out that the physical regime in such a

Rydberg-atom system is different from either Rydberg blockade or antiblockade. Our choice of parameters gives the antiblockade condition $\omega = V_{jt}$ [58], as the first sideband of the modulation field offsets the control-target RRI. Dynamically, however, a single Rydberg atom can be excited, similar to the Rydberg blockade [53–56]. In this peculiar regime one-step implementation of multiqubit gates distinguish from other schemes, such as Rydberg-antiblockade gates whose gate times increase exponentially with N [58] and multiple-step Rydberg-blockade gates [25, 37, 59]. Besides, the present multiqubit gate scheme experiences less errors caused by atomic decay and motional dephasing, compared with the recent Rydberg-blockade adiabatic multiqubit gate scheme [28] where a control atom remains excited to accumulate a slow adiabatic 2π pulse on the target.

Pulse engineering scheme.—NHQC gates based on rectangular pulses are usually sensitive to errors in the pulse area, e.g., amplitude Ω_t and duration T of the operation field [21, 22, 33]. As an example, we first calculate fidelities of a CNOT gate by replacing the gate time with $T + \delta T$ or Rabi frequency with $\Omega_t + \delta\Omega_t$, shown in Fig. 3(a). The infidelity increases drastically when errors in the laser parameter (T or Ω_t) are large.

The error tolerance of $(N+1)$ -QHG can be improved by pulse engineering. We control the laser pulse with a time-dependent operation field $\Omega_t(t)$ and a time-dependent detuning $\Delta(t)$ between the transition $|B\rangle_t \leftrightarrow |A\rangle_t$. The full Hamiltonian now becomes $\hat{H}_I + \Delta(t)|r\rangle_t\langle r|$. Under condition $\max\{|\Delta(t)|, |\Omega_t(t)|\} \ll \Omega_m/2$, we can obtain an effective Hamiltonian of the $(N+1)$ atoms, $\hat{H}''_I = \left(\bigotimes_j^N |1\rangle_j\langle 1|\right) \otimes \hat{H}''_t$ with $\hat{H}''_t = \frac{\Omega_t(t)}{2}\hat{\sigma}_t^x + \frac{\Delta(t)}{2}\hat{\sigma}_t^z$. Explicitly, the operation field is given in the following form [38]

$$\begin{aligned} \Omega_t(t) &= \dot{\alpha}\sqrt{1 + \lambda^2 \sin^2 \alpha}, \\ \Delta(t) &= -\lambda\dot{\alpha} \cos \alpha - \frac{\dot{\lambda} \sin \alpha + \lambda\dot{\alpha} \cos \alpha}{1 + \lambda^2 \sin^2 \alpha}, \end{aligned} \quad (4)$$

where α is a piecewise function $\alpha = 12\pi t'^2/T^2 - 16\pi t'^3/T^3$ with $t' = t$ for $t \in [0, T/2]$ or $t' = t - T/2$ for $t \in (T/2, T]$, and $\lambda = 2 + 2a_1 \cos(2\alpha) + 4a_2 \cos(4\alpha)$ with the optimal parameters $a_1 = 0.28$ and $a_2 = -0.12$ corresponding to a gate time $\max\{\Omega_t(t)\}T/2\pi = 2.85$. Piecewise phases are $\varphi_0 = 0$ and $\varphi_1 = \pi + \phi$ during $t \in [0, T/2]$ while $\varphi_0 = \pi + \gamma$ and $\varphi_1 = \gamma + \phi$ during $t \in (T/2, T]$. This set of parameters results to geometric evolution as shown on the Bloch sphere in Fig. 1(d). More importantly, the robustness of the gate is significantly improved with pulses in Eq. (4) and $\Omega' \equiv \max\{|\Omega_t(t)|\}/2\pi = 0.25 \text{ MHz}$, as shown in Fig. 3(a). With the engineered pulse, the fidelity is hardly reduced by introducing errors to $\Omega_t(t)$ when $|\delta\Omega_t/\Omega'| \leq 0.1$.

Robust multiqubit holonomic gates.—To demonstrate the robustness of OHQC, we will examine fluctuations that are close to experimental situation. First,

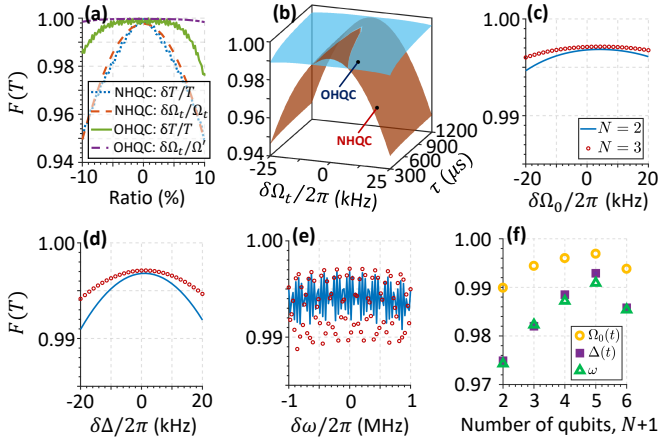


FIG. 3. (a) CNOT gate fidelity versus relative errors in T and Ω_t . The fidelity is improved significantly with OHQC. (b) CNOT gate fidelities when varying Ω_t and Rydberg lifetime τ . The NHQC has high fidelities when both $\delta\Omega_t$ and τ are small. OHQC achieves better fidelities when $\tau > 900 \mu\text{s}$ or $|\delta\Omega_t|/2\pi > 7.5 \text{ kHz} = 0.03\Omega'$. When implementing C_N -NOT gates with $N = 2$ and $N = 3$, fidelities are affected by errors in (c) $\Omega_0(t)$, (d) $\Delta(t)$, and (e) ω , respectively. (f) C_N -NOT gate fidelity for different N . The relative errors in $\Omega_0(t)$, $\Delta(t)$, and ω are 5%.

finite Rydberg lifetime τ will be considered. In this case, dynamics of the gate is governed by a Markov master equation [38]. Second, we assume that the driving fields, involving parameters $\Omega_0(t)$ [the same as $\Omega_1(t)$], $\Delta(t)$, and ω , suffer systematic errors. Finally, we will take into account of fluctuations of interatomic separations, causing fluctuations to the RRI.

In Fig. 3(b), fidelities of a CNOT gate with varying $\delta\Omega_t$ and Rydberg lifetime τ are shown. Our simulations show that gate fidelities of OHQC are always higher than that of NHQC when $\tau > 900 \mu\text{s}$ or $|\delta\Omega_t|/2\pi > 7.5 \text{ kHz} = 0.03\Omega'$. When $\tau = 1 \text{ ms}$ (see SM [38]), average fidelities for two- and three-qubit controlled- $\tilde{U}_t(\theta, \phi, \gamma)$ of OHQC are better than 0.995.

We next turn to investigate effects due to fluctuations of parameters $\Omega_0(t)$, $\Delta(t)$, and ω . Fluctuations of $\Omega_0(t)$ affect gate fidelities weakly. As shown in Figure 3(c), fidelities with $N = 2$ and $N = 3$ are always over 0.9946 when $|\delta\Omega_0| \leq 2\pi \times 20 \text{ kHz} = 0.11 \times \max[\Omega_0(t)]$. Errors in $\Delta(t)$ are of complicated dynamics, which not only affect the gate time slightly, but also cause unwanted dynamical phases. We eliminate the dynamical phase through a spin-echo operation [22], which switches the sign of the dynamical phase halfway during the gate operation. Then the gate fidelity is slightly reduced [Fig. 3(d)] by $|\delta\Delta/2\pi| \leq 20 \text{ kHz}$. The gate fidelity oscillates with varying $\delta\omega$, as shown in Fig. 3(e). Here the lowest fidelity is almost 0.99 when $|\delta\omega|/2\pi \leq 1 \text{ MHz}$.

The gate fidelity increases with N as the number $(2^N - 2)$ of invariant computational product states increases [see Figs. 3(c) and (d)]. When further increasing

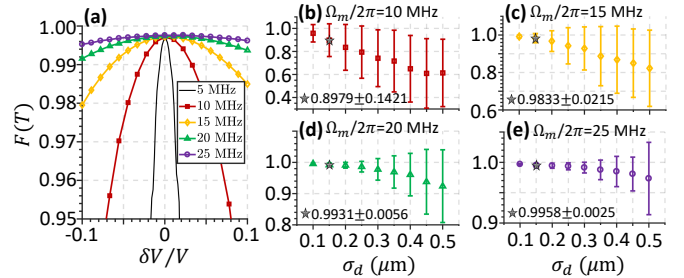


FIG. 4. (a) Fidelities of a CNOT gate when considering errors in the RRI. The gate becomes robust with increasing Ω_m . (b)–(e) fidelities versus σ_d with increasing $\Omega_m/2\pi$. The fidelity in general decreases with increasing σ_d . Each point is the average value of 1000 results from canonically distributed values of the interatomic distance. Error bars denote standard deviations.

N , however, the fidelity reaches a maxima and then decreases [Fig. 3(f)]. When N is too large, the multiqubit condition is not strictly satisfied (e.g. $V_{jt} \gg \sqrt{M}\Omega_m$ as \sqrt{M} is large). In the example shown in Fig. 3(f), C_4 -NOT gate has the highest fidelity.

We now investigate effects of fluctuations of the RRI strength V (through distance d_i) by focusing on CNOT gates. In Fig. 4(a) fidelities of the CNOT gate versus $\delta V/V$ are shown. The result shows that the gate becomes more robust when increasing Ω_m . To describe the fluctuations of V , d_i follows a quasi-one-dimensional Gaussian with a standard deviation σ_d [36]. Larger σ_d generally leads to smaller fidelities with larger variations [see Figs. 4(b)–(e)]. The fidelity can be increased by increasing Ω_m . However, when Ω_m is too large, the fidelity may be reduced [38]. This can be mitigated with smaller σ_d , achieved with state-of-the-art cooling and trapping method. For example using parameters from experiment [44], the standard deviations are estimated to be $\sigma_d \approx 0.14 \mu\text{m}$. The fidelity is better than 0.99 with $\Omega_m/2\pi \gtrsim 20 \text{ MHz}$.

Conclusion.—We have presented an approach to realizing fast and robust $(N+1)$ -qubit holonomic gates. A unique advantage is that both universal ($N=0, 1$) and multiqubit ($N \geq 2$) gates can be implemented within the same gate time. Using Rydberg atom arrays, the parameter regime to implement the $(N+1)$ -qubit holonomic gate is identified. We have demonstrated that the gates are robust against errors in the laser fields and interatomic interactions. It is found that the tolerance of the respective gates is much greater than that of nonadiabatic holonomic quantum computation.

Besides neutral Rydberg atoms, trapped Rydberg ions [60] are another candidate to realize the holonomic gates proposed in this work. Moreover, the $(N+1)$ -qubit holonomic gates can be implemented alternatively with superconducting circuits [38], which has unique advantages, e.g. immune to atomic spatial arrangement. Our study

opens a new route to build robust and error-tolerant multiqubit holonomic gates, which find applications in scalable quantum computation and simulation of many-body models.

We acknowledge supports from National Natural Science Foundation of China (NSFC) (11675046, 11804308, 21973023), Program for Innovation Research of Science in Harbin Institute of Technology (A201412), Postdoctoral Scientific Research Developmental Fund of Heilongjiang Province (LBH-Q15060), and National Basic Research Program of China (2014CB340203). W. L. acknowledges support from the EPSRC through Grant No. EP/R04340X/1 via the QuantERA project “ERyQSenS”, the UKIERI-UGC Thematic Partnership (IND/CONT/G/16-17/73), and the Royal Society through the International Exchanges Cost Share award No. IEC\NSFC\181078.

* jsong@hit.edu.cn

† slsu@zzu.edu.cn

‡ weibin.li@nottingham.ac.uk

[1] M. V. Berry, *Proc. R. Soc. Lond. A* **392**, 45 (1984)

[2] F. Wilczek and A. Zee, *Phys. Rev. Lett.* **52**, 2111 (1984)

[3] P. J. Leek, J. M. Fink, A. Blais, R. Bianchetti, M. Göppel, J. M. Gambetta, D. I. Schuster, L. Frunzio, R. J. Schoelkopf, and A. Wallraff, *Science* **318**, 1889 (2007).

[4] S. Filipp, J. Klepp, Y. Hasegawa, C. Plonka-Spehr, U. Schmidt, P. Geltenbort, and H. Rauch, *Phys. Rev. Lett.* **102**, 030404 (2009)

[5] P. Zanardi and M. Rasetti, *Phys. Lett. A* **264**, 94 (1999).

[6] L.-M. Duan, J. I. Cirac, and P. Zoller, *Science* **292**, 1695 (2001).

[7] L.-A. Wu, P. Zanardi, and D. A. Lidar, *Phys. Rev. Lett.* **95**, 130501 (2005)

[8] E. Sjöqvist, D. M. Tong, L. M. Andersson, B. Hessmo, M. Johansson, and K. Singh, *New J. Phys.* **14**, 103035 (2012).

[9] G. F. Xu, J. Zhang, D. M. Tong, E. Sjöqvist, and L. C. Kwek, *Phys. Rev. Lett.* **109**, 170501 (2012).

[10] G. F. Xu, C. L. Liu, P. Z. Zhao, and D. M. Tong, *Phys. Rev. A* **92**, 052302 (2015).

[11] Z.-P. Hong, B.-J. Liu, J.-Q. Cai, X.-D. Zhang, Y. Hu, Z. D. Wang, and Z.-Y. Xue, *Phys. Rev. A* **97**, 022332 (2018).

[12] A. A. Abdumalikov Jr, J. M. Fink, K. Juliusson, M. Pechal, S. Berger, A. Wallraff, and S. Filipp, *Nature* **496**, 482 (2013).

[13] G. Feng, G. Xu, and G. Long, *Phys. Rev. Lett.* **110**, 190501 (2013).

[14] C. Zu, W.-B. Wang, L. He, W.-G. Zhang, C.-Y. Dai, F. Wang, and L.-M. Duan, *Nature* **514**, 72 (2014).

[15] S. Arroyo-Camejo, A. Lazariev, S. W. Hell, and G. Balasubramanian, *Nat. Commun.* **5**, 4870 (2014).

[16] Y. Sekiguchi, N. Niikura, R. Kuroiwa, H. Kano, and H. Kosaka, *Nat. Photonics* **11**, 309 (2017).

[17] B. B. Zhou, P. C. Jerger, V. O. Shkolnikov, F. Heremans, G. Burkard, and D. D. Awschalom, *Phys. Rev. Lett.* **119**, 140503 (2017).

[18] H. Li, Y. Liu, and G. Long, *Sci. China Phys. Mech. Astron.* **60**, 080311 (2017).

[19] Y. Xu, W. Cai, Y. Ma, X. Mu, L. Hu, T. Chen, H. Wang, Y. P. Song, Z.-Y. Xue, Z.-q. Yin, and L. Sun, *Phys. Rev. Lett.* **121**, 110501 (2018).

[20] Z. Zhang, P. Z. Zhao, T. Wang, L. Xiang, Z. Jia, P. Duan, D. M. Tong, Y. Yin, and G. Guo, *New J. Phys.* **21**, 073024 (2019).

[21] B.-J. Liu, X.-K. Song, Z.-Y. Xue, X. Wang, and M.-H. Yung, *Phys. Rev. Lett.* **123**, 100501 (2019).

[22] T. Yan, B.-J. Liu, K. Xu, C. Song, S. Liu, Z. Zhang, H. Deng, Z. Yan, H. Rong, K. Huang, M.-H. Yung, Y. Chen, and D. Yu, *Phys. Rev. Lett.* **122**, 080501 (2019).

[23] D. Maslov and G. Dueck, *Electron. Lett.* **39**, 1790 (2003).

[24] M. Müller, I. Lesanovsky, H. Weimer, H.P. Büchler, and P. Zoller, *Phys. Rev. Lett.* **102**, 170502 (2009).

[25] L. Isenhower, M. Saffman, and K. Mølmer, *Quantum Inf. Process.* **10**, 755 (2011).

[26] E. A. Martinez, T. Monz, D. Nigg, P. Schindler, and R. Blatt, *New J. Phys.* **18**, 063029 (2016).

[27] S. E. Rasmussen, K. Groenland, R. Gerritsma, K. Schoutens, and N. T. Zinner, *Phys. Rev. A* **101**, 022308 (2020).

[28] M. Khazali and K. Mølmer, *Phys. Rev. X* **10**, 021054 (2020).

[29] H. Weimer, M. Müller, I. Lesanovsky, P. Zoller, and H. P. Büchler, *Nat. Phys.* **6**, 382 (2010).

[30] A. Keesling, A. Omran, H. Levine, H. Bernien, H. Pichler, S. Choi, R. Samajdar, S. Schwartz, P. Silvi, S. Sachdev, P. Zoller, M. Endres, M. Greiner, V. Vuletić, and M. D. Lukin, *Nature* **568**, 207 (2019).

[31] F. M. Gambetta, W. Li, F. Schmidt-Kaler, and I. Lesanovsky, *Phys. Rev. Lett.* **124**, 043402 (2020).

[32] F. M. Gambetta, C. Zhang, M. Hennrich, I. Lesanovsky, and W. Li, *Phys. Rev. Lett.* **125**, 133602 (2020).

[33] S.-B. Zheng, C.-P. Yang, and F. Nori, *Phys. Rev. A* **93**, 032313 (2016).

[34] D. P. DiVincenzo, *Phys. Rev. A* **51**, 1015 (1995)

[35] H. Labuhn, D. Barredo, S. Ravets, S. de Léséleuc, T. Macrì, T. Lahaye, and A. Browaeys, *Nature* **534**, 667 (2016).

[36] T. M. Graham, M. Kwon, B. Grinkemeyer, Z. Marra, X. Jiang, M. T. Lichtman, Y. Sun, M. Ebert, and M. Saffman, *Phys. Rev. Lett.* **123**, 230501 (2019).

[37] H. Levine, A. Keesling, G. Semeghini, A. Omran, T. T. Wang, S. Ebadi, H. Bernien, M. Greiner, V. Vuletić, H. Pichler, and M. D. Lukin, *Phys. Rev. Lett.* **123**, 170503 (2019).

[38] See Supplemental Material for illustrations of the effective dynamics for the many-body model, a holonomic transformation $\hat{U}_t(\theta, \phi, \gamma)$, two-photon processes for Rydberg pumping, optimal pulse engineering, a lower limit of coupling strength between two control qubits, average fidelities of optimized $(N+1)$ -QHG, fidelity evolution of a CNOT gate with different Ω_m , and the many-body model in superconducting circuit, which includes Refs. [17,22,36,37,39–52].

[39] Y. Xu, Z. Hua, T. Chen, X. Pan, X. Li, J. Han, W. Cai, Y. Ma, H. Wang, Y. P. Song, Z.-Y. Xue, and L. Sun, *Phys. Rev. Lett.* **124**, 230503 (2020).

[40] F. Kleißler, A. Lazariev, and S. Arroyo-Camejo,

npj Quantum Inf. **4**, 49 (2018).

[41] D. Barredo, H. Labuhn, S. Ravets, T. Lahey, A. Browaeys, and C. S. Adams, Phys. Rev. Lett. **114**, 113002 (2015).

[42] H. Levine, A. Keesling, A. Omran, H. Bernien, S. Schwartz, A. S. Zibrov, M. Endres, M. Greiner, V. Vuletić, and M. D. Lukin, Phys. Rev. Lett. **121**, 123603 (2018).

[43] A. Omran, H. Levine, A. Keesling, G. Semeghini, T. T. Wang, S. Ebadi, H. Bernien, A. S. Zibrov, H. Pichler, S. Choi, J. Cui, M. Rossignolo, P. Rembold, S. Montangero, T. Calarco, M. Endres, M. Greiner, V. Vuletić and M. D. Lukin, Science **365**, 570 (2019).

[44] H. Jo, Y. Song, M. Kim, and J. Ahn, Phys. Rev. Lett. **124**, 033603 (2020).

[45] X. L. Zhang, L. Isenhower, A. T. Gill, T. G. Walker, and M. Saffman, Phys. Rev. A **82**, 030306(R) (2010).

[46] L. Isenhower, E. Urban, X. L. Zhang, A. T. Gill, T. Henage, T. A. Johnson, T. G. Walker, and M. Saffman, Phys. Rev. Lett. **104**, 010503 (2010).

[47] A. Vepsäläinen, S. Danilin, and G. S. Paraoanu, Sci. Adv. **5**, eaau5999 (2019).

[48] D. Daems, A. Ruschhaupt, D. Sugny, and S. Guérin, Phys. Rev. Lett. **111**, 050404 (2013).

[49] A. Ruschhaupt, X. Chen, D. Alonso, and J. G. Muga, New J. Phys. **14**, 093040 (2012).

[50] M. A. Nielsen, Phys. Lett. A **303**, 249 (2002).

[51] C. Song, K. Xu, H. Li, Y.-R. Zhang, X. Zhang, W. Liu, Q. Guo, Z. Wang, W. Ren, J. Hao, H. Feng, H. Fan, D. Zheng, D.-W. Wang, H. Wang, and S.-Y. Zhu, Science **365**, 574 (2019).

[52] R. Barends, et al., Phys. Rev. Lett. **123**, 210501 (2019).

[53] D. Jaksch, J. I. Cirac, P. Zoller, S. L. Rolston, R. Côté, and M. D. Lukin, Phys. Rev. Lett. **85**, 2208 (2000).

[54] M. Saffman, T. G. Walker, and K. Mølmer, Rev. Mod. Phys. **82**, 2313 (2010).

[55] A. Browaeys and T. Lahaye, Nat. Phys. **16**, 132 (2020).

[56] M. D. Lukin, M. Fleischhauer, R. Cote, L. M. Duan, D. Jaksch, J. I. Cirac, and P. Zoller, Phys. Rev. Lett. **87**, 037901 (2001).

[57] S. Basak, Y. Chougale, and R. Nath, Phys. Rev. Lett. **120**, 123204 (2018).

[58] T. H. Xing, X. Wu, and G. F. Xu, Phys. Rev. A **101**, 012306 (2020).

[59] X.-F. Shi, Phys. Rev. Appl. **9**, 051001 (2018).

[60] C. Zhang, F. Pokorny, W. Li, G. Higgins, A. Pöschl, I. Lesanovsky, and M. Hennrich, Nature **580**, 345 (2020).

Supplementary material for “Error-tolerant multiqubit holonomic entangling gates”

In this Supplemental Material we provide additional details on the effective dynamics for the many-body model, a holonomic transformation $\hat{U}_t(\theta, \phi, \gamma)$, two-photon processes for Rydberg pumping, optimal pulse engineering, a lower limit of coupling strength between two control qubits, average fidelities of optimized $(N+1)$ -QHG, fidelity evolution of a CNOT gate with different Ω_m , and the many-body model in superconducting circuit.

EFFECTIVE DYNAMICS OF THE MANY-BODY MODEL

In the interaction picture, the Hamiltonian of the many-body model reads ($\hbar = 1$ hereinafter)

$$\hat{H}_i = \hat{H}_c + \hat{H}_t + \hat{H}_{\text{Ising}}, \quad (\text{S1})$$

with $\hat{H}_c = \sum_{j=1}^N \Omega_c(t) \hat{\sigma}_j^x / 2$, $\hat{H}_t = \Omega_t(t) \hat{\sigma}_t^x / 2$, and $\hat{H}_{\text{Ising}} = \sum_{j>k=1}^N (J_{jk} \hat{n}_j \hat{n}_k + J_{jt} \hat{n}_j \hat{n}_t)$, where the subscript j (k) denotes the j -th (k -th) control qubit, the subscript t the target qubit, J_{jk} (J_{jt}) the interqubit coupling strength, and $\hat{n} \equiv (\hat{\sigma}^z + \hat{I})/2$. $\hat{\sigma}^x$, $\hat{\sigma}^y$, and $\hat{\sigma}^z$ are usual Pauli operators, and \hat{I} the identity operator, on $\{|A\rangle, |B\rangle\}$. The control qubits are described by collective quantum states $|\psi_c^K\rangle \equiv |B\rangle^K |A\rangle^{M-K}$ with integers $0 \leq K \leq M \leq N$, in which the numbers of qubits in $|D\rangle$, $|B\rangle$, and $|A\rangle$ are $(N-M)$, K , and $(M-K)$, respectively. The control field couples $|\psi_c^K\rangle$ and $|\psi_c^{K-1}\rangle$ ($K \geq 1$). The composite basis of the control and target qubits are $|\chi_1^K\rangle \equiv |\psi_c^K\rangle |B\rangle_t$, $|\chi_2^K\rangle \equiv |\psi_c^K\rangle |A\rangle_t$, $|\chi_3^K\rangle \equiv |\psi_c^{K-1}\rangle |B\rangle_t$, and $|\chi_4^K\rangle \equiv |\psi_c^{K-1}\rangle |A\rangle_t$. State $|\chi_l^K\rangle$ has an energy of the Ising-like interaction energy, $E_l^K = \sum_{j>k=1}^{M-K+\delta_{l3}+\delta_{l4}} [J_{jk} + (\delta_{l2} + \delta_{l4}) J_{jt}]$, where $\delta_{ll'}$ is the Kronecker delta function and the subscript j (k) denotes the j -th (k -th) entry over the control qubits in $|A\rangle$.

It is convenient to study the system into the rotating frame with respect to the Ising-like interactions using the transformation $\hat{\mathcal{U}} = \exp(i\hat{H}_{\text{Ising}}t)$. In this new frame, the Hamiltonian of the $(N+1)$ -qubit system takes the form

$$\hat{H} = \sum_{M=0}^N \sum_{K=0}^M \left[\frac{\sqrt{K} \Omega_c(t)}{2} \left(\hat{S}_{31}^K e^{it\Delta_{31}^K} + \hat{S}_{42}^K e^{it\Delta_{42}^K} \right) + \frac{\Omega_t(t)}{2} \left(\hat{S}_{21}^K e^{it\Delta_{21}^K} + \hat{S}_{43}^K e^{it\Delta_{43}^K} \right) \right] + \text{H.c.}, \quad (\text{S2})$$

where $\hat{S}_{jk}^K = \hat{S}_{kj}^{K\dagger} = |\chi_j^K\rangle \langle \chi_k^K|$ with $\{j, k\} = \{1, 2, 3, 4\}$ is the collective transition operator, and $\Delta_{jk}^K = -\Delta_{kj}^K = E_j^K - E_k^K$ is the detuning. When considering strong interqubit couplings that can result in $|\Delta_{jk}^K| \gg \max\{|\Omega_c(t)|, |\Omega_t(t)|\}$ for

any nonzero $(M - K)$, only the terms of $K = M$ remain in consideration, with $E_1^M = E_2^M = E_3^M = 0$ and $E_4^M = J_{jt}$, and the Hamiltonian (S2) becomes

$$\hat{H}' = \sum_{M=0}^N \left[\frac{\sqrt{M}\Omega_c(t)}{2} \left(\hat{S}_{31}^M + \hat{S}_{42}^M e^{itJ_{jt}} \right) + \frac{\Omega_t(t)}{2} \left(\hat{S}_{21}^M + \hat{S}_{43}^M e^{itJ_{jt}} \right) \right] + \text{H.c.} \quad (\text{S3})$$

We set an identical control-target interqubit coupling strength $J_{jt} = J_0$ and an amplitude-modulated control field $\Omega_c(t) = \Omega_m \cos \omega t$, with Ω_m being the amplitude and ω the modulation frequency. We choose $|\omega| = |J_0|$, for example $\omega = J_0$, so the Hamiltonian (S3) becomes

$$\hat{H}'' = \sum_{M=0}^N \left\{ \frac{\sqrt{M}\Omega_m}{4} \left[\hat{S}_{31}^M \left(e^{itJ_0} + e^{-itJ_0} \right) + \hat{S}_{42}^M \left(e^{2itJ_0} + 1 \right) \right] + \frac{\Omega_t(t)}{2} \left(\hat{S}_{21}^M + \hat{S}_{43}^M e^{itJ_0} \right) \right\} + \text{H.c.} \quad (\text{S4})$$

When the condition $|J_0| \gg \sqrt{N}\Omega_m/4, \max\{|\Omega_t(t)|/2\}$ is considered, the highly oscillating terms concerning \hat{S}_{31}^M and \hat{S}_{43}^M can be neglected under the rotating wave approximation. Therefore, the interference between the amplitude modulation of the control field and the target-control interqubit coupling gives rise to an effective Hamiltonian

$$\hat{\mathcal{H}}_{\text{eff}} = \sum_{M=0}^N \left[\frac{\sqrt{M}\Omega_m}{4} \left(\hat{S}_{24}^M + \hat{S}_{42}^M \right) + \frac{\Omega_t(t)}{2} \left(\hat{S}_{12}^M + \hat{S}_{21}^M \right) \right]. \quad (\text{S5})$$

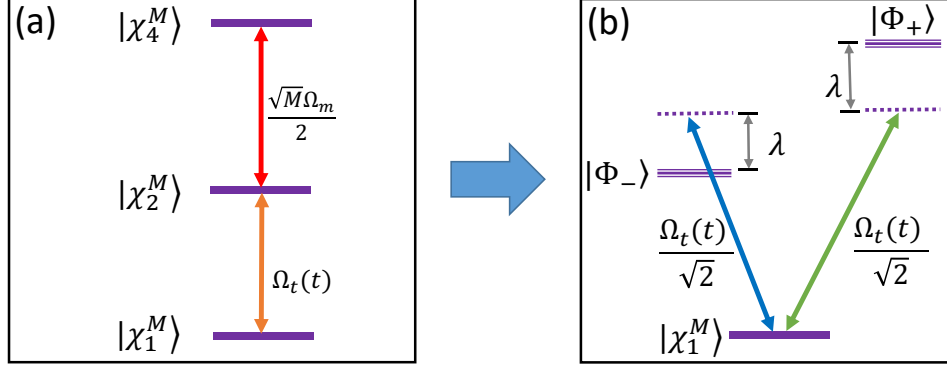


FIG. 5. (a) Three-level interaction with $M \neq 0$ in Eq. (S5). (b) Three-level interaction in (a) represented on the dressed-state basis. $\lambda = \sqrt{M}\Omega_m/4$.

Hamiltonian $\hat{\mathcal{H}}_{\text{eff}}$ involves a series of M -dependent three-level systems containing transitions $|\chi_1^M\rangle \leftrightarrow |\chi_2^M\rangle$ and $|\chi_2^M\rangle \leftrightarrow |\chi_4^M\rangle$ with Rabi frequencies $\Omega_t(t)$ and $\sqrt{M}\Omega_m/2$, respectively, as shown in Fig. 5(a). We consider the diagonalization of the interaction $\hat{h}_1 = \sqrt{M}\Omega_m/4 \left(\hat{S}_{24}^M + \hat{S}_{42}^M \right)$, i.e., $\hat{h}_1 \rightarrow \hat{h}'_1 = \sqrt{M}\Omega_m/4 (|\Phi_+\rangle\langle\Phi_+| - |\Phi_-\rangle\langle\Phi_-|)$, yielding two dressed states $|\Phi_{\pm}\rangle \equiv (|\chi_2^M\rangle \pm |\chi_4^M\rangle)/\sqrt{2}$. Then in the representation of the dressed states, after moving to \hat{h}'_1 frame with a unitary transformation $\exp(i\hat{h}'_1 t)$ Eq. (S5) becomes

$$\hat{\mathcal{H}}'_{\text{eff}} = \sum_{M=0}^N \left[\frac{\Omega_t(t)}{2\sqrt{2}} |\chi_1^M\rangle \left(\langle\Phi_+| e^{-i\lambda t} + \langle\Phi_-| e^{i\lambda t} \right) \right] + \text{H.c.}, \quad (\text{S6})$$

for which the schematic diagram of transitions is shown in Fig. 5(b). In order to suppress the evolution of the three-level systems for all $M \neq 0$, here we set $\Omega_m/2 \gg \max\{|\Omega_t(t)|\}$, such that the transitions of $M \neq 0$ have a much longer time scale than that for the transitions of $M = 0$. Therefore, we can neglect the terms with $M \neq 0$, and the final effective Hamiltonian is

$$\hat{\mathcal{H}}_{\text{e}} = \left(\bigotimes_j^N |D\rangle_j \langle D| \right) \otimes \hat{H}_t. \quad (\text{S7})$$

Only when all control qubits populate in $|D\rangle$ will the operation field on the target qubit work. Otherwise, the evolution of all the $(N + 1)$ qubits is frozen.

SINGLE-LOOP IMPLEMENTATION OF SINGLE-QUBIT HOLONOMIC GATES

A three-level system, as shown in Fig. 6(a), involves two computational states $|0\rangle$ and $|1\rangle$ and an intermediated auxiliary state $|A\rangle$. The transitions $|0\rangle \leftrightarrow |A\rangle$ and $|1\rangle \leftrightarrow |A\rangle$ are driven by using two slightly detuned classical fields with different Rabi frequencies $\Omega_0(t)$ and $\Omega_1(t)$ and phases φ_0 and φ_1 , respectively, and the same time-dependent frequency detuning $\Delta(t)$. When we consider $\Omega_0(t)$ and $\Omega_1(t)$ have identical time-dependent envelopes $\Omega(t) = \sqrt{\Omega_0^2(t) + \Omega_1^2(t)}$ with $\Omega_0(t)/\Omega_1(t) = \tan(\theta/2)$ being a constant. The interaction-picture Hamiltonian of this three-level system is

$$\begin{aligned}\hat{H}_I &= \frac{\hbar}{2} [\Omega_0(t)e^{i\varphi_0}|0\rangle\langle A| + \Omega_1(t)e^{i\varphi_1}|1\rangle\langle A| + \text{H.c.}] + \hbar\Delta(t)|A\rangle\langle A| \\ &= \frac{\hbar}{2} [\Omega(t)e^{i\varphi_0}|B\rangle\langle A| + \text{H.c.}] + \hbar\Delta(t)|A\rangle\langle A|.\end{aligned}\quad (\text{S8})$$

where $|B\rangle \equiv \sin(\theta/2)|0\rangle - \cos(\theta/2)e^{i\phi}|1\rangle$, with $\phi \equiv \varphi_1 - \varphi_0 - \pi$. There is also an orthogonal state $|D\rangle \equiv \cos(\theta/2)|0\rangle + \sin(\theta/2)e^{i\phi}|1\rangle$ which is decoupled to $|B\rangle$ and $|A\rangle$, as shown in Fig. 6(b).

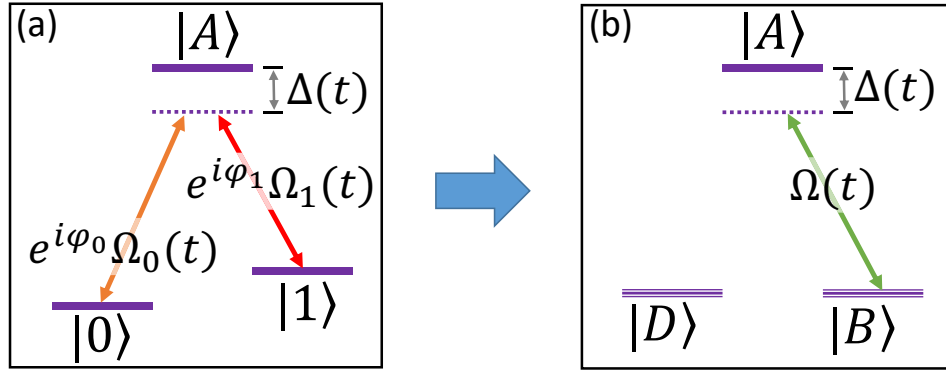


FIG. 6. (a) Three-level model for the single-loop implementation of holonomic arbitrary single-qubit gates. (b) Effective three-level model of (a). $|B\rangle \equiv \sin(\theta/2)|0\rangle - \cos(\theta/2)e^{i\phi}|1\rangle$ and $|D\rangle \equiv \cos(\theta/2)|0\rangle + \sin(\theta/2)e^{i\phi}|1\rangle$.

Through pulse engineering, the state transfer $|B\rangle \mapsto |A\rangle$ during $t \in [0, T/2]$ and $|A\rangle \mapsto |B\rangle$ during $t \in (T/2, T]$ can be achieved without accumulating any dynamical phase (See Sec.). When we set the phases $\varphi_0 = 0$ and $\varphi_1 = \pi + \phi$ for $t \in [0, T/2]$ while switch them into $\varphi_0 = \pi + \gamma$ and $\varphi_1 = \gamma + \phi$ for $t \in (T/2, T]$, an extra geometric phase γ on $|B\rangle$ is obtained, for which the system experiences a single-loop geometric evolution [See the Bloch sphere in the inset box of Fig. 1(d) in the main text]. Switching of laser field phases has been realized experimentally when implementing non-adiabatic non-Abelian [19], shortcut-to-adiabatic non-Abelian [22], non-adiabatic Abelian [39], and shortcut-to-adiabatic Abelian [40] universal geometric gates. The evolution operator $|D\rangle\langle D| + e^{i\gamma}|B\rangle\langle B|$ is expressed by the computational states $\{|0\rangle, |1\rangle\}$ as

$$\begin{aligned}\hat{U}(\theta, \phi, \gamma) &= \begin{bmatrix} \cos^2 \frac{\theta}{2} + e^{i\gamma} \sin^2 \frac{\theta}{2} & \frac{1}{2}e^{-i\phi_1}(e^{i\gamma} - 1) \sin \frac{\theta}{2} \\ \frac{1}{2}e^{i\phi_1}(e^{i\gamma} - 1) \sin \frac{\theta}{2} & e^{i\gamma} \cos^2 \frac{\theta}{2} + \sin^2 \frac{\theta}{2} \end{bmatrix} \\ &= \exp(i\frac{\gamma}{2}) \exp(-i\frac{\gamma}{2}\mathbf{n} \cdot \boldsymbol{\sigma}),\end{aligned}\quad (\text{S9})$$

where $\mathbf{n} = (\sin \theta \cos \phi, \sin \theta \sin \phi, \cos \theta)$ and $\boldsymbol{\sigma} = (\hat{\sigma}^x, \hat{\sigma}^y, \hat{\sigma}^z)$ are the standard Pauli operators:

$$\hat{\sigma}^x = \begin{bmatrix} 0 & 1 \\ 1 & 0 \end{bmatrix}, \quad \hat{\sigma}^y = \begin{bmatrix} 0 & -i \\ i & 0 \end{bmatrix}, \quad \hat{\sigma}^z = \begin{bmatrix} 1 & 0 \\ 0 & -1 \end{bmatrix}.\quad (\text{S10})$$

With different choices of $\{\theta, \phi, \gamma\}$, arbitrary single-qubit gates can be achieved. Take several frequently-used ones as examples,

$$\begin{aligned}X &= \hat{U}(\frac{\pi}{2}, 0, \pi) = \begin{bmatrix} 0 & 1 \\ 1 & 0 \end{bmatrix}, \quad Y = \hat{U}(\frac{\pi}{2}, \frac{\pi}{2}, \pi) = \begin{bmatrix} 1 & -i \\ i & 1 \end{bmatrix}, \\ Z &= \hat{U}(0, 0, \pi) = \begin{bmatrix} 1 & 0 \\ 0 & -1 \end{bmatrix}, \quad H = \hat{U}(\frac{\pi}{4}, 0, \pi) = \frac{1}{\sqrt{2}} \begin{bmatrix} 1 & 1 \\ 1 & -1 \end{bmatrix}, \\ E &= \hat{U}(\frac{\pi}{2}, 0, \frac{\pi}{2}) = \frac{1}{2} \begin{bmatrix} 1+i & 1-i \\ 1-i & 1+i \end{bmatrix}, \quad T = \hat{U}(0, 0, \pi/4) = \begin{bmatrix} 1 & 0 \\ 0 & e^{i\pi/4} \end{bmatrix}.\end{aligned}\quad (\text{S11})$$

TWO-PHOTON RYDBERG PUMPING

In order to implementing holonomic gates with Rydberg atoms, the Rydberg pumping from a ground state to a Rydberg state can be achieved by a two-photon process [37, 41–44] in Rb atoms or a single-photon process [36] in Cs atoms. Here we consider related energy levels of ^{87}Rb atoms $|0\rangle \equiv |5S_{1/2}, F = 1, m_F = 1\rangle$, $|1\rangle \equiv |5S_{1/2}, F = 2, m_F = 2\rangle$, and $|r\rangle \equiv |100S_{1/2}, m_J = 1/2, m_I = 3/2\rangle$ with $C_6/2\pi = 56.197 \text{ THz } \mu\text{m}^6$. The excitation of a Rydberg state in ^{87}Rb atoms with a principal quantum numbers near 100 has been demonstrated [45, 46]. Then assisted by an intermediate state $|p\rangle = |5p_{3/2}\rangle$, the atomic transition $|0(1)\rangle = |5S_{1/2}, F = 1(2), m_F = 1(2)\rangle \leftrightarrow |r\rangle = |100S_{1/2}\rangle$ can be achieved through a two-photon process, as shown in Fig. 7.

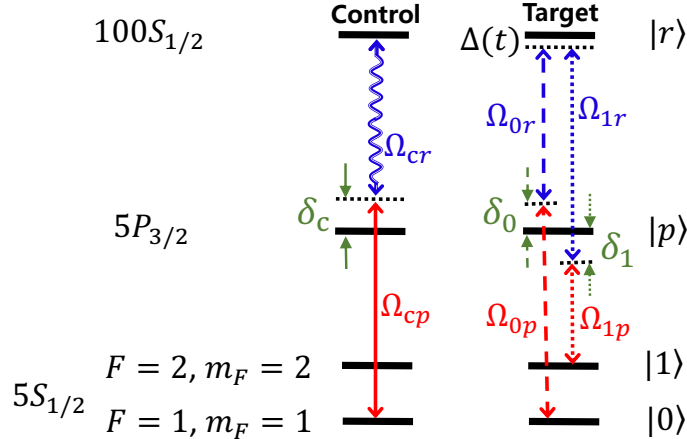


FIG. 7. Schematic diagram for the two-photon Rydberg excitations in ^{87}Rb atoms.

Each transition is achieved by two laser fields. For the control atoms, one field is imposed for the optical excitation $|0\rangle \leftrightarrow |p\rangle$ with Rabi frequency Ω_{cp} and a blue detuning δ_c , and the other for the Rydberg excitation $|p\rangle \leftrightarrow |r\rangle$ with Rabi frequency Ω_{cr} and a red detuning δ_c . The field on the control atoms for $|p\rangle \leftrightarrow |r\rangle$ is modulated in amplitude $\Omega_{1r} = \tilde{\Omega}_m \cos \omega t$. For the target atom, one field is imposed for the optical excitation $|0\rangle \leftrightarrow |p\rangle$ ($|1\rangle \leftrightarrow |p\rangle$) with (time-dependent) Rabi frequency $\Omega_{0p}(t)$ [$\Omega_{1p}(t)$] and a blue (red) detuning δ_0 (δ_1), and the other for the Rydberg excitation $|p\rangle \leftrightarrow |r\rangle$ with Rabi frequency Ω_{0r} (Ω_{1r}) and a red (blue) detuning $\delta_0 + \Delta(t)$ [$\delta_1 - \Delta(t)$]. The detunings for $|0\rangle \leftrightarrow |p\rangle$ and $|1\rangle \leftrightarrow |p\rangle$ are of opposite signs so as to avoid the effective coupling between two ground states. $\Delta(t)$ is a small time-dependent detuning for pulse engineering, while δ_c , δ_0 , and δ_1 are so large that the intermediate state $|p\rangle$ can be adiabatically eliminated and the Rydberg pumping from ground states is achieved.

The quantities used directly for holonomic gates are $\Omega_m = \tilde{\Omega}_m \Omega_{cp}/2\delta_c$, $\Omega_0(t) = \Omega_{0r} \Omega_{0p}(t)/2\delta_0$, and $\Omega_1(t) = \Omega_{1r} \Omega_{1p}(t)/2\delta_1$. When we set the distance from the target atom to the control atoms as $9.6 \mu\text{m}$ that are within the range of the van der Waals interaction, corresponding to a strength $V_{jt}/2\pi = 71.79 \text{ MHz}$. To satisfy the condition $V_{jt} \gg \Omega_m/4 \gg \max\{\Omega_t(t)/2, \Delta(t)/2\}$ with $\Omega_t(t) = \sqrt{\Omega_0^2(t) + \Omega_1^2(t)}$, we assume $\Omega_{cp} = \Omega_m = 2\pi \times 200 \text{ MHz}$, $\delta_c = 2\pi \times 2 \text{ GHz}$, which indicates $\Omega_m/2\pi = 10 \text{ MHz}$. For the Rydberg pumping of the target atom, we can adopt smaller Rabi frequencies or larger detunings to make $\Delta(t) \sim \max\{\Omega_t(t)\} = 2\pi \times 0.25 \text{ MHz}$. It should also be noted that in addition to the two-photon effective coupling from a ground state to the Rydberg state, there are Stark-shift terms $\Omega_{cp}^2/4\delta_c |0\rangle_c \langle 0|$, $\Omega_m^2 \cos^2 \omega t / 4\delta_c |r\rangle_c \langle r|$, $\Omega_{0p}^2/4\delta_0 |0\rangle_t \langle 0|$, $-\Omega_{1p}^2/4\delta_1 |1\rangle_t \langle 1|$, and $(\Omega_{0r}^2/4\delta_0 - \Omega_{1r}^2/4\delta_1) |r\rangle_t \langle r|$. These unwanted energy shifts can be offset by imposing additional lasers to drive the off-resonant transitions between the related states and some auxiliary states so as to induce opposite Stark shifts. Alternatively, these unwanted energy shifts can also be eliminated through phase corrections [47].

OPTIMIZED PULSE ENGINEERING

Using Hamiltonian $\hat{H}'_t = [\Omega_t(t)\hat{\sigma}_t^x + \Delta(t)\hat{\sigma}_t^z]/2$, we transfer the full population from $|B\rangle_t$ first to $|r\rangle_t$ during $t \in [0, T/2]$ and then back to $|B\rangle_t$ during $t \in (T/2, T]$, with T being the gate time. In the following, we mainly discuss the population transfer from $|B\rangle_t$ to $|r\rangle_t$, because the inverse process is based on the same theory. During the state transfer from $|B\rangle_t$ to $|r\rangle_t$, a solution of the time-dependent Schrödinger equation $i\partial|\psi\rangle/\partial t = \hat{H}'_t|\psi\rangle$ can be parametrized as a superposition $|\psi_0(t)\rangle = e^{-i\eta/2} [e^{i\beta/2} \cos(\alpha/2) |B\rangle_t + e^{-i\beta/2} \sin(\alpha/2) |r\rangle_t]$ [48], for which the time

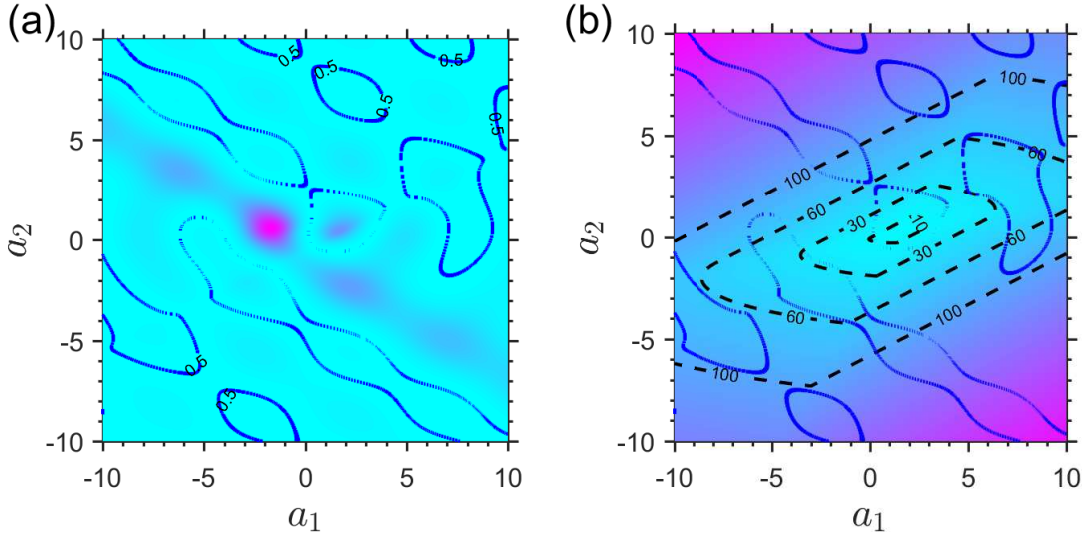


FIG. 8. (a) Error sensitivity S versus a_1 and a_2 . (b) $T \max\{\Omega_t(t)\}/2$ versus a_1 and a_2 . Blue lines are 0.5 contour lines of S . Black dashed lines in (b) are contour lines of $T \max\{\Omega_t(t)\}/2$ with different values.

dependence symbol “(t)” of $\alpha(t)$, $\beta(t)$, and $\eta(t)$ is omitted for simplicity. There is also an orthogonal solution $|\psi_1(t)\rangle = e^{i\eta/2} [e^{i\beta/2} \sin(\alpha/2)|B\rangle_t - e^{-i\beta/2} \cos(\alpha/2)|r\rangle_t]$ such that $\langle\psi_1(t)|\psi_0(t)\rangle = 0$. Inserting $|\psi_0(t)\rangle$ and $|\psi_1(t)\rangle$ into the Schrödinger equation, $\Omega_t(t)$ and $\Delta(t)$ are related to α and β , as

$$\Omega_t(t) = \frac{\dot{\alpha}}{\sin \beta}, \quad \Delta(t) = \dot{\beta} - \dot{\alpha} \cot \alpha \cot \beta. \quad (\text{S12})$$

At the same time, the global phase $\eta = \int_0^t \dot{\alpha}(t') \cot \beta(t') / \sin \alpha(t') dt'$ can be obtained, and $\eta(T) = 0$ is supposed to be satisfied so as to ensure a null dynamical phase. We assume that the evolution follows $|\psi_0(t)\rangle$, and thus the boundary conditions $\alpha(0) = 0$ and $\alpha(T/2) = \pi$ are supposed to be met for completing the state transfer $|B\rangle_t \mapsto |r\rangle_t$.

We introduce a systematic error δX into an ideal parameter X , yielding an actual parameter $(X + \delta X)$. Our goal is to design a pair of $\Omega_t(t)$ and $\Delta(t)$ such that the holonomic gates are insensitive to systematic errors in the gate time T and the pulse amplitude $\Omega_t(t)$. For errors in the gate time, $\Omega_t(t)$ and $\Delta(t)$ can be designed to be softly turned on and off, so that a moderate surplus or deficiency in the pulse duration has little effect on the pulse area. When $\delta\Omega_t$ is taken into account, it leads to a perturbation-containing Hamiltonian $\hat{\mathcal{H}}_t = \hat{H}'_t + \hat{\mathcal{H}}_r$ with $\hat{\mathcal{H}}_r = \frac{\delta\Omega_t}{2} \hat{\sigma}_t^x$. Then using the perturbation theory and keeping the final state to the second order, we obtain a perturbed population of $|r\rangle_t$ at $t = T/2$, as $P_r(T/2) \simeq 1 - \left| \int_0^{T/2} dt \langle\psi_1(t)|\hat{\mathcal{H}}_r|\psi_0(t)\rangle \right|^2$. Then we define a quantity $S \equiv -\frac{1}{2} \left. \frac{\partial^2 P_r}{\partial \delta\Omega_t^2} \right|_{\delta\Omega_t=0}$ to measure the sensitivity of P_r to the systematic error in $\Omega_t(t)$ [49]. Substituting the expressions of $|\psi_0(t)\rangle$ and $|\psi_1(t)\rangle$ into $P_r(T/2)$, the systematic error sensitivity can be calculated out

$$S = \frac{1}{4} \left| \int_0^{T/2} dt e^{-i\eta} (\cos \alpha \cos \beta + i \sin \beta) \right|^2. \quad (\text{S13})$$

For rendering holonomic gates to hold strong tolerance to $\delta\Omega_t$, S is supposed to be as small as possible, which needs pulse engineering with suitable forms of α , β , and η . According to $\alpha(0) = 0$ and $\alpha(T/2) = \pi$, α can be designed with a polynomial ansatz as $\alpha = 12\pi t^2/T^2 - 16\pi t^3/T^3$. Then we choose $\eta = 2\alpha + a_1 \sin(2\alpha) + a_2 \sin(4\alpha)$ such that the dynamical phase is absent at $t = T/2$, and a_1 and a_2 are to be determined so as to minimize S . The forms of α and η give $\beta = \cos^{-1}(\lambda \sin \alpha / \sqrt{1 + \lambda^2 \sin^2 \alpha})$ with $\lambda = 2 + 2a_1 \cos(2\alpha) + 4a_2 \cos(4\alpha)$, so

$$\begin{aligned} \Omega_t(t) &= \dot{\alpha} \sqrt{1 + \lambda^2 \sin^2 \alpha}, \\ \Delta(t) &= -\lambda \dot{\alpha} \cos \alpha - \frac{\dot{\lambda} \sin \alpha + \lambda \dot{\alpha} \cos \alpha}{1 + \lambda^2 \sin^2 \alpha}. \end{aligned} \quad (\text{S14})$$

In order to achieve a small sensitivity to systematic errors and a short gate time, in Figs. 8(a) and 8(b) we plot numerically S and $T \max\{\Omega_t(t)\}/2$, respectively, with varying a_1 and a_2 . We find that in the region of $T \max\{\Omega_t(t)\}/2 < 30$

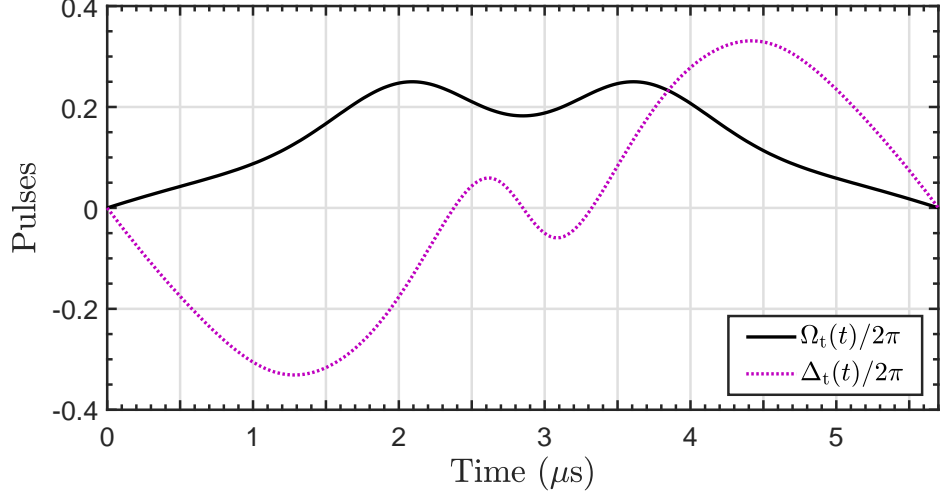


FIG. 9. Pulse forms with $\max\{\Omega_t(t)\}/2\pi = 0.25$ MHz, $a_1 = 0.28$ and $a_2 = -0.12$.

there exists a very small region of $S < 0.5$, which indicates a trend that a small error sensitivity costs a longer gate time. However, there are still points guaranteeing $S < 0.5$ and $T \max\{\Omega_t(t)\}/2 < 10$. For example, $a_1 = 0.28$ and $a_2 = -0.12$ give $S = 0.3$ and $T \max\{\Omega_t(t)\} = 17.9$. This gate time is three times longer than that (2π) of non-adiabatic holonomic gates.

With the trade-off between the robustness and the speed of implementing holonomic gates, we pick up $a_1 = 0.28$ and $a_2 = -0.12$ that can ensure a short gate time $\max\{\Omega_t(t)\}T/2\pi = 2.85$ and a small systematic-error sensitivity $S = 0.3$. Based on Eq. (S14), the pulse forms can be determined, as shown in Fig. 9, with which the state transfer $|B\rangle_t \mapsto |r\rangle_t$ can be achieved with an enhanced tolerance against the systematic error in $\Omega_t(t)$. An identical process can be performed again to transfer the population from $|r\rangle_t$ back to $|B\rangle_t$.

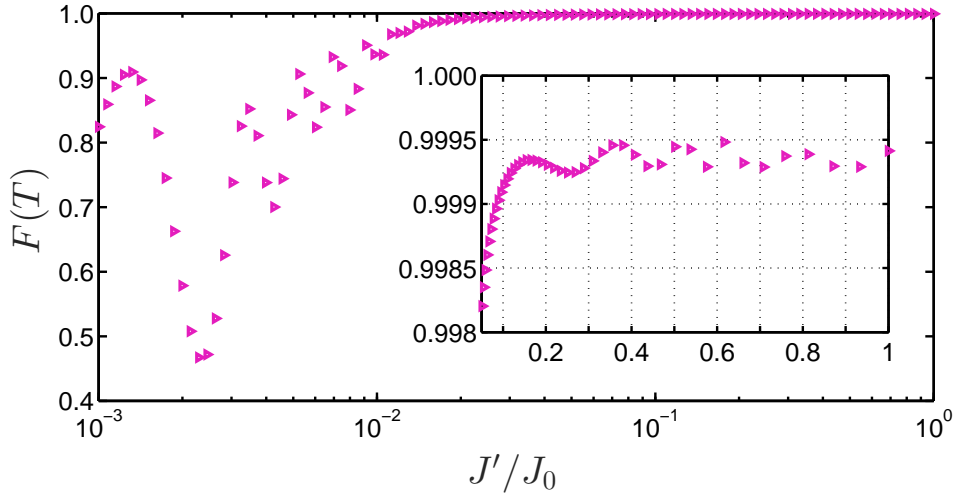


FIG. 10. $F(T)$ of performing a Toffoli gate versus the ratio J'/J_0 where J' is the coupling strength between the two control qubits while J_0 is that between the target qubit and each of control qubits. $\tilde{\Omega} \equiv \max\{\Omega_t(t)\} = 17.9/T$, $\Omega_m = 50\tilde{\Omega}$, and $J_0 = 500\tilde{\Omega}$.

LOWER LIMIT OF COUPLING STRENGTH BETWEEN CONTROL QUBITS

For $N \geq 2$, only one of control qubits is allowed to be excited, for a Rydberg-atom system which is exactly corresponding to the Rydberg blockade among the control atoms. In the context of Rydberg atoms, the blockade

radius is $r_b = (C_6/\Omega)^{1/6}$ [44] where C_6 is the van der Waals interaction coefficient and Ω is the strength of Rydberg pumping, which implies a lower limit of coupling strength between control qubits in our work, i.e., $J_{\min} \sim \Omega_m$. To make the situation more clear, we pick $N = 2$ and solve numerically the Schrödinger equation $i\partial|\Psi(t)\rangle/\partial t = [\hat{H}_I + \Delta(t)|r\rangle_t\langle r|]\langle\Psi(t)\rangle$ to obtain the fidelity of a target state $|\Psi_t\rangle$ after performing a Toffoli gate on an initial state $|\Psi(t=0)\rangle = \bigotimes_j^2 (|0\rangle_j - |1\rangle_j) \otimes (|0\rangle_t - |1\rangle_t)/2\sqrt{2}$. \hat{H}_I is Eq. (3) in the main text, and the fidelity is defined by $F(t) = |\langle\Psi_t|\Psi(t)\rangle|^2$. Based on the optimized pulse engineering, in Fig. 10 we plot $F(T)$ versus the ratio J'/J_0 where J' is the coupling strength between the two control qubits while J_0 is that between the target qubit and each of control qubits. When $J' \gtrsim \Omega_m = 0.1J_0$, the fidelity $F(T)$ can remain over 0.999, which shows that $J_{\min} \sim \Omega_m$ can be treated as the lower limit of coupling strength between control qubits in our work.

AVERAGE FIDELITIES OF $(N+1)$ -QUBIT HOLONOMIC GATES

The evolution of the many-body master equation can be numerically simulated based on the fourth-order variable step-size Runge-Kutta algorithm

$$\dot{\hat{\rho}} = -i[\hat{H}_I, \hat{\rho}] - \frac{1}{2} \sum_{k=1}^{N+1} \sum_{j=0,1,g} \left(\hat{\mathcal{L}}_{jk}^\dagger \hat{\mathcal{L}}_{jk} \hat{\rho} - 2\hat{\mathcal{L}}_{jk} \hat{\rho} \hat{\mathcal{L}}_{jk}^\dagger + \hat{\rho} \hat{\mathcal{L}}_{jk}^\dagger \hat{\mathcal{L}}_{jk} \right), \quad (\text{S15})$$

in which the Lindblad operator $\hat{\mathcal{L}}_{jk} \equiv \sqrt{\gamma_j} |j\rangle_k \langle r|$ describes decay of the k -th atom from the Rydberg state $|r\rangle$ to a ground state $|j\rangle$ with a decay rate γ_j , for which an additional ground state $|g\rangle$ is introduced to denote those Zeeman magnetic sublevels out of the computational states $|0\rangle$ and $|1\rangle$. For convenience, we assume that decay rates from a Rydberg state of ^{87}Rb atoms into the eight Zeeman ground states are identical, so $\gamma_0 = \gamma_1 = 1/8\tau$ and $\gamma_g = 3/4\tau$ with τ being the lifetime of the Rydberg state.

Here we take the two- and three-qubit holonomic gates as examples, and show the average fidelities to verify the arbitrariness of an initial state. The average fidelity is defined based on a trace-preserving operator, as [50]

$$\bar{F}(\varepsilon, \hat{U}) = \frac{\sum_{j=1}^{4^{N+1}} \text{tr} [\hat{U} \hat{u}_j^\dagger \hat{U}^\dagger \varepsilon(\hat{u}_j)] + l^2}{l^2(l+1)}, \quad (\text{S16})$$

where $\hat{u}_j = \bigotimes_k^4 \hat{\sigma}_k$ is the tensor of Pauli matrices $\hat{\sigma}_k \in \{\hat{I}, \hat{\sigma}^x, \hat{\sigma}^y, \hat{\sigma}^z\}$ on computational states $\{|0\rangle, |1\rangle\}$, and $l = 2^{N+1}$ for an $(N+1)$ -qubit gate. $\varepsilon(\hat{u}_j)$ is a trace-preserving quantum operation obtained through solving the master equation. We show average fidelities of various two- and three-qubit controlled- $\hat{U}_t(\theta, \phi, \gamma)$ gates in Fig. 11(a) and Fig. 11(b), respectively. The evolutionary trends of the average fidelity for different gates are dependent of the value of γ , and the two- and three-qubit gates can be achieved with average fidelities over 0.995.

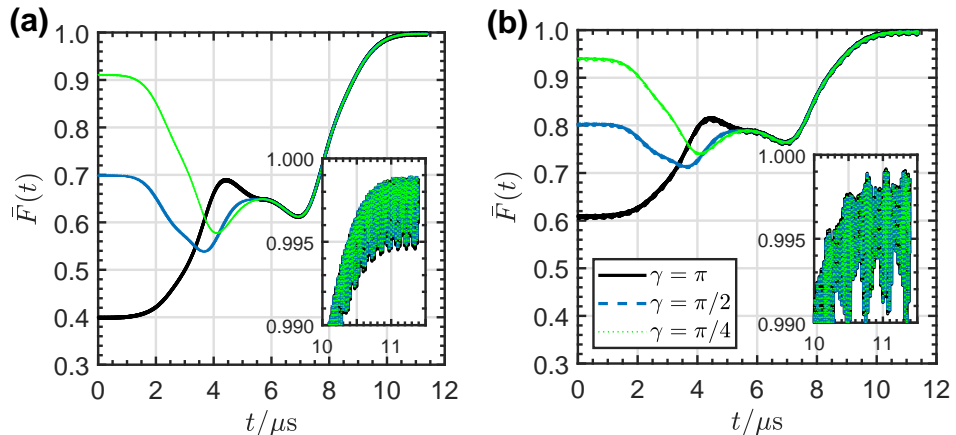


FIG. 11. Trace-preserving-operator-based average fidelities of controlled $\hat{U}_t(\theta, \phi, \gamma)$ gates with different values of γ . (a) Two-qubit gates. (b) Three-qubit gates. $\tau = 1$ ms.

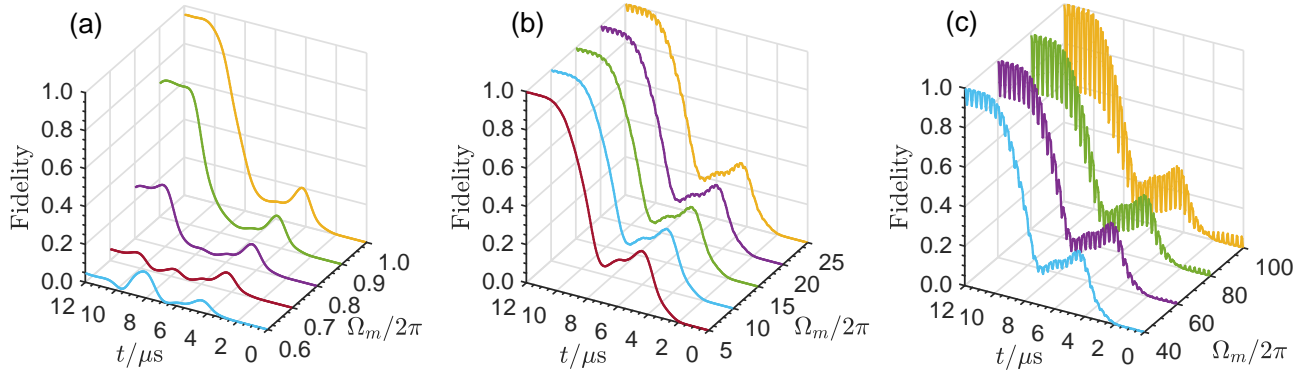
FIDELITY EVOLUTION OF A CNOT GATE WITH DIFFERENT Ω_m 

FIG. 12. Fidelity evolution in the Rydberg-atom system of a CNOT gate on an initial state $(|0\rangle_1 - |1\rangle_1) \otimes (|0\rangle_t - |1\rangle_t)/2$ with (a) small Ω_m , (b) relatively suitable Ω_m , and (c) large Ω_m .

For the value region of Ω_m , on one hand, the condition $\Omega_m/2 \gg |\Omega_t(t)|$ is needed for our scheme to exclude the dynamics concerning the control qubits populating in $|B\rangle$, which is pretty crucial for realizing quantum gates. On the other hand, under the condition $J_0 \gg \sqrt{N}\Omega_m/4$, off-resonant terms in Eq. (S4), including $[\frac{\Omega_m}{4}\hat{S}_{31}^M(e^{itJ_0} + e^{-itJ_0}) + \text{H.c.}]$, $[\frac{\Omega_m}{4}\hat{S}_{42}^M e^{2itJ_0} + \text{H.c.}]$, and $[\frac{\Omega_t(t)}{2}\hat{S}_{43}^M e^{itJ_0} + \text{H.c.}]$, have trivial influence on the full dynamics. In Figs. 12(a)–(c), we plot fidelity evolution of a CNOT gate in the Rydberg-atom system with Ω_m being in different value regions. For a small Ω_m in Fig. 12(a), the dynamics is spoiled for realizing a high-fidelity CNOT gate. Figure 12(b) shows a relatively suitable region of Ω_m that gives high gate fidelities at the end time and slight oscillations during the evolution. When Ω_m is enhanced beyond a certain extent, the unwanted dynamics induced by the off-resonant terms will emerge and even spoil the desired dynamics. In Fig. 12(c), a high $F(T)$ of the CNOT gate may be achieved, but there are intense oscillations during the evolution which make the gate tolerance to timing error very fragile.

MANY-BODY MODEL IN SUPERCONDUCTING CIRCUIT

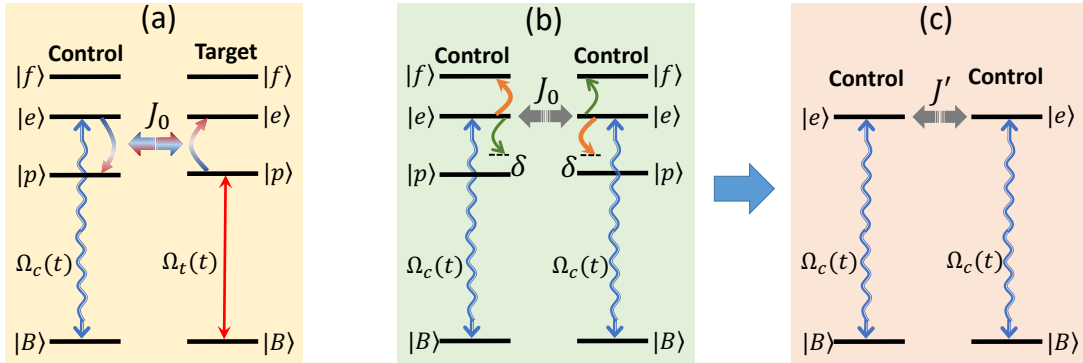


FIG. 13. (a) Level structures of a pair of interacting control and target superconducting qubits. (b) Level structures of two interacting control qubits. (c) Effective coupling between two control qubits with the effective coupling strength $J' = 2J_0^2/\delta$. The decoupled state $|D\rangle$ for each qubit is omitted for simplicity.

Superconducting artificial atoms are an alternative promising platform of constructing the proposed many-body model. As the coupling strength between two superconducting qubits can be independent of their spatial distributions, the many-body model in superconducting circuit can be not limited by the spatial arrangement of qubits. Here we present a proposal for implementing the $(N+1)$ -qubit gate with superconducting artificial atoms.

We consider $(N+1)$ superconducting artificial-atom qubits coupled capacitively or inductively to each other through exchange interactions [51, 52]. The considered level structures of control and target qubits are shown in Fig. 13(a),

where auxiliary states are $|e\rangle$ and $|p\rangle$ for control and target qubits, respectively. Five levels are taken into account, for which the two computational states $|0\rangle$ and $|1\rangle$ that form the dressed states $|B\rangle$ and $|D\rangle$ are supposed to be chosen as long-lived lower-energy states, for example two ground states of double-trap potential in a flux qubit. Classical microwave fields are applied to drive the transitions $|B\rangle \leftrightarrow |e\rangle$ and $|B\rangle \leftrightarrow |p\rangle$ of the control qubits and the target qubit, respectively, with Rabi frequencies $\Omega_c(t)$ and $\Omega_t(t)$. Three higher levels are responsible for interqubit couplings. Between the j -th control qubit and the target qubit, the coupling is achieved via the resonant exchange interaction $|e\rangle_j|p\rangle_t \leftrightarrow |p\rangle_j|e\rangle_t$ with strength J_0 . However, among target qubits, as shown in Fig. 13(b), couplings can be achieved via off-resonant exchange interactions $|e\rangle_j|e\rangle_k \leftrightarrow |p\rangle_j|f\rangle_k + |f\rangle_j|p\rangle_k$ with strength J'_0 and detuning δ due to the anharmonicity of energy levels. When the anharmonicity is large sufficiently, $\delta \gg J'_0$, the exchange interactions between two control qubits will not occur but induce an energy shift of the pair state $|e\rangle_j|e\rangle_k$, which then causes an effective coupling between the two qubits with an effective coupling strength $J' = 2J'_0/\delta$, as shown in Fig. 13(c).

The Hamiltonian describing the couplings among the $(N + 1)$ qubits, corresponding to the many-body Ising-like Hamiltonian, can be written as

$$\hat{H}_0 = \sum_{j>k=1}^N J_0 (|E_+\rangle_{jt}\langle E_+| - |E_-\rangle_{jt}\langle E_-|) + J' |ee\rangle_{jk}\langle ee|, \quad (\text{S17})$$

with $|E_{\pm}\rangle_{jt} \equiv (|e\rangle_j|p\rangle_t \pm |p\rangle_j|e\rangle_t)/\sqrt{2}$. Then we consider the condition $J' \gtrsim \Omega_m$ such that only one of the control qubits can be excited (see Sec.). Therefore, the control field drives the M -dependent transition $|\Psi_c^M\rangle \leftrightarrow |\Psi_c^{M-1}\rangle|e\rangle_j$ ($0 < M < N$), with $|\Psi_c^M\rangle \equiv |D\rangle^{N-M}|B\rangle^M$ in which the numbers of qubits in $|D\rangle$ and $|B\rangle$ are $(N - M)$ and M , respectively. Normalized $|\Psi_c^{M-1}\rangle|e\rangle_j$ denotes a state where the j -th one of control qubits in $|B\rangle$ is excited into $|e\rangle$. We define $|\vartheta_1^M\rangle \equiv |\Psi_c^M\rangle|B\rangle_t$, $|\vartheta_2^M\rangle \equiv |\Psi_c^M\rangle|p\rangle_t$, $|\vartheta_3^M\rangle \equiv |\Psi_c^{M-1}\rangle|e\rangle_j|B\rangle_t$, and $|\vartheta_{\pm}^M\rangle \equiv |\Psi_c^{M-1}\rangle|E_{\pm}\rangle_{jt}$, according to which $|\Psi_c^{M-1}\rangle|e\rangle_j|p\rangle_t = (|\vartheta_+^M\rangle + |\vartheta_-^M\rangle)/\sqrt{2}$. Then after moving into the frame with respect to \hat{H}_0 , the Hamiltonian of the interacting $(N + 1)$ qubits is written as

$$\begin{aligned} \hat{H}_1 = & \sum_{M=0}^N \left\{ \frac{\sqrt{M}\Omega_c(t)}{2} \left[|\vartheta_3^M\rangle\langle\vartheta_1^M| + \frac{1}{\sqrt{2}} \left(e^{itJ_0}|\vartheta_+^M\rangle + e^{-itJ_0}|\vartheta_-^M\rangle \right) \langle\vartheta_2^M| \right] \right. \\ & \left. + \frac{\Omega_t(t)}{2} \left[|\vartheta_2^M\rangle\langle\vartheta_1^M| + \frac{1}{\sqrt{2}} \left(e^{itJ_0}|\vartheta_+^M\rangle + e^{-itJ_0}|\vartheta_-^M\rangle \right) \langle\vartheta_3^M| \right] \right\} + \text{H.c..} \end{aligned} \quad (\text{S18})$$

When we set $\Omega_c = \Omega_m \cos(\omega t)$ and $|\omega| = |J_0| \gg \sqrt{N}\Omega_m/4, \max\{|\Omega_t(t)|/2\}$, the amplitude-modulated control field will interfere with the coupling between the target and control qubits. After neglecting the highly oscillating terms with the rotating wave approximation, \hat{H}_1 becomes

$$\hat{H}_2 = \sum_{M=0}^N \frac{\sqrt{M}\Omega_m}{4} |\Psi_c^{M-1}\rangle|e\rangle_j|p\rangle_t\langle\vartheta_2^M| + \frac{\Omega_t(t)}{2} |\vartheta_2^M\rangle\langle\vartheta_1^M| + \text{H.c.}, \quad (\text{S19})$$

which has the same form as Eq. (S5). Therefore, under the condition $\Omega_m/2 \gg \max\{|\Omega_t(t)|\}$, an identical effective Hamiltonian can be obtained, i.e., $\hat{\mathcal{H}}_e = \left(\bigotimes_j^N |D\rangle_j\langle D| \right) \otimes \hat{H}_t$, which shows that the many-body model for implementing $(N + 1)$ -qubit holonomic gates is constructed with superconducting artificial atoms.

To identify the validity of the many-body model for implementing $(N + 1)$ -qubit holonomic gates, in Fig. 14 with the optimized pulses we simulate the evolution of the fidelity for the target state after a CNOT gate or a Toffoli gate performed on the initial state $|\Psi(0)\rangle = \bigotimes_j^N (|0\rangle_j - |1\rangle_j) \otimes (|0\rangle_t - |1\rangle_t)/\sqrt{2}^{N+1}$ by solving numerically the Schrödinger equation with respect to the full $(N + 1)$ -qubit Hamiltonian

$$\begin{aligned} \hat{H} = & \sum_{j>k=1}^N J_0 \left(|pe\rangle_{jt}\langle ep| + |pf\rangle_{jk}\langle ee|e^{i\delta t} + |fp\rangle_{jk}\langle ee|e^{i\delta t} + \text{H.c.} \right) \\ & + \left(\sum_{j=1}^N \frac{\Omega_c(t)}{2} |0\rangle_j\langle e| + \sum_{l=0,1} \frac{\Omega_l(t)}{2} e^{i\varphi_l} |l\rangle_t\langle p| + \text{H.c.} \right) + \Delta(t) |p\rangle_t\langle p|. \end{aligned} \quad (\text{S20})$$

We pick a set of parameters [$J_0 = \omega = 2\pi \times 50$ MHz, $\delta = 2\pi \times 400$ MHz, $\Omega_m = 2\pi \times 7.5$ MHz, $\max\{\Omega_t(t)\} = 2\pi \times 0.25$ MHz]. The fidelity curves of the target state can reach over 0.995 for performing both the CNOT and Toffoli gates, which proves that the many-body model with superconducting artificial atoms is valid for implementing

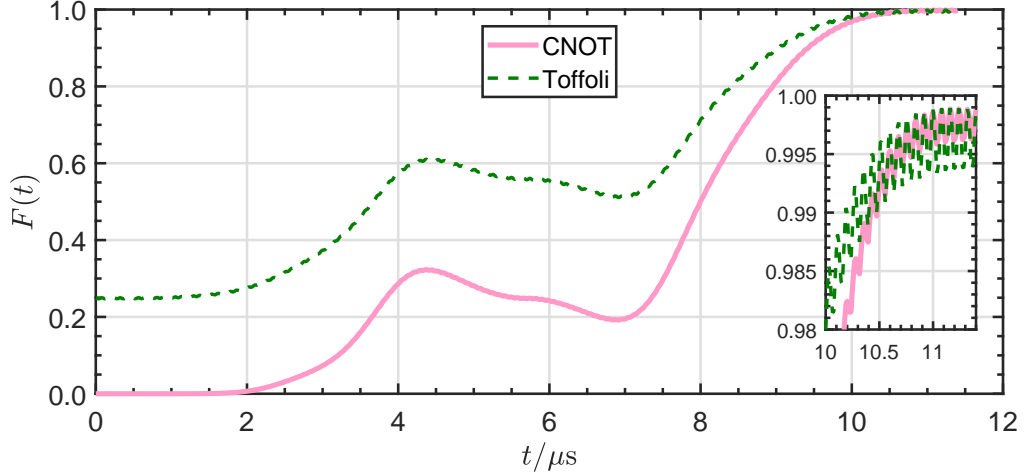


FIG. 14. Fidelity evolution of performing a CNOT gate ($N = 1$) or a Toffoli gate ($N = 2$) on the initial state $|\Psi(0)\rangle = \bigotimes_j^N (|0\rangle_j - |1\rangle_j) \otimes (|0\rangle_t - |1\rangle_t)/\sqrt{2}^{N+1}$. $J_0 = \omega = 2\pi \times 50$ MHz, $\delta = 2\pi \times 400$ MHz, $\Omega_m = 2\pi \times 7.5$ MHz, and $\max\{\Omega_t(t)\} = 2\pi \times 0.25$ MHz.

($N + 1$)-qubit holonomic gates. The infidelity $1 - F(T)$ is induced by factors including the imperfect rotating-wave approximation (not large enough J_0 and ω), a not large enough anharmonicity δ , “blockade errors” among control qubits (a not large enough J'), and a not large enough Ω_m . These infidelity factors are difficult to avoid thoroughly because of the trade-off among these parameters when considering experimental feasibility.